Particle dynamics in horizontal stirred bed reactors characterized by single-photon emission radioactive particle tracking

van der Sande, P. Christian; Wagner, Evert C.; de Mooij, Jack; Meesters, Gabrie M.H.; van Ommen, J. Ruud

DOI
10.1016/j.cej.2024.149100

Publication date
2024

Document Version
Final published version

Published in
Chemical Engineering Journal

Citation (APA)
van der Sande, P. C., Wagner, E. C., de Mooij, J., Meesters, G. M. H., & van Ommen, J. R. (2024). Particle dynamics in horizontal stirred bed reactors characterized by single-photon emission radioactive particle tracking. *Chemical Engineering Journal*, *482*, Article 149100. https://doi.org/10.1016/j.cej.2024.149100

Chemical Engineering Journal 482 (2024) 149100

Contents lists available at ScienceDirect

Chemical Engineering Journal

journal homepage: www.elsevier.com/locate/cej

Particle dynamics in horizontal stirred bed reactors characterized by single-photon emission radioactive particle tracking

P. Christian van der Sande *, Evert C. Wagner, Jack de Mooij, Gabrie M.H. Meesters, J. Ruud van Ommen

Delft University of Technology, Department of Chemical Engineering, van der Maasweg 9, Delft, 2629HZ, The Netherlands

ARTICLE INFO

Keywords:
Horizontal stirred bed reactors
Polypropylene
Radioactive particle tracking
Multiphase reactors
Reactor optimization

ABSTRACT

Horizontal stirred bed reactors are widely used in the commercial manufacturing of polypropylene. However, a comprehensive understanding of the particle dynamics in horizontal stirred bed reactors remains elusive, primarily due to the lack of detailed experimental data. In this work, we studied the influence of operating parameters on the particle flow dynamics in a laboratory-scale horizontal stirred bed reactor using single-photon emission radioactive particle tracking. The results show that the general solids flow behavior is strongly affected by both the agitator rotation speed and reactor fill level. Operation at low rotation speed and low fill level results in solids flow with poor radial and circumferential distribution due to internal bed circulation. On the contrary, at increased rotation speeds and fill levels, solids motion throughout the bed is continuous resulting in excellent solids distribution. The solids circulation was found to increase for both an increase in rotation speed and reactor fill level. The axial dispersion coefficient, on the other hand, shows a linear relation with the rotation speed, but no conclusive relation between the axial dispersion coefficient and the reactor fill level was found.

1. Introduction

Polypropylene (PP) is the second-most produced polyolefin resin globally, trailing only polyethylene. PP is recognized as a versatile material with robust mechanical properties, thermal stability, and excellent chemical resistance and therefore widely used in food packaging, automotive, healthcare, textile, and electronics industries [1,2]. The global PP market is projected to experience sustained growth due to the increasing demand for efficient food packaging solutions and the incorporation of high-quality plastics in automotive manufacturing [3].

Among various PP manufacturing methods, gas-phase catalyzed polymerization has gained significant commercial importance [4]. In particular, the utilization of horizontal stirred bed reactors (HSBRs) in the gas-phase Innovene PP process has proven to be a successful approach for efficient and scalable PP production [5–9]. The HSBR offers distinct advantages for propylene polymerization, ensuring excellent gas-phase mixing and precise control of reaction parameters.

The HSBR is a cylindrical reactor with a series of paddles attached to a central shaft as illustrated in Fig. 1. At the front end of the HSBR micron-sized Ziegler–Natta supported catalyst particles are continuously introduced. Gaseous propylene monomers are injected at the bottom of the reactor and polymerize on the active sites of the catalyst surface via a coordination-insertion mechanism. The gas velocity is carefully controlled to prevent fluidization of the bed and maintain a sub-fluidized state. The mildly agitated PP powder is maintained at a constant inventory while the polymerization progresses and the particles grow to a final size ranging from 100 to 5000 μm [10]. The volume increase due to particle growth pushes the powder toward the opposite end of the reactor where it is continuously discharged.

In gas-phase polymerization reactors, operational issues can arise if the process is not adequately operated with respect to particle movement. Besides reduced production capacity and product quality, a significant issue encountered in the reactors is the agglomeration of polyolefin particles [11]. In the Innovene PP process, agglomeration may arise due to insufficient heat dissipation, as a result of poor solids circulation. Insufficient heat dissipation during the process can lead to elevated surface temperatures of polymer particles, potentially reaching the softening temperature or even surpassing the melting temperature of the polymer, resulting in the local formation of agglomerates or lumps. Agglomeration can significantly impair reactor efficiency by obstructing the discharging pipeline, disrupting the heat exchange balance, causing deviations from the normal flow pattern, and in severe cases occupying a substantial portion of the reactor volume, leading to an unscheduled shutdown of the plant and incurring substantial financial penalties [12].

* Corresponding author.
E-mail addresses: P.C.vanderSande@tudelft.nl (P.C. van der Sande), J.R.vanOmmen@tudelft.nl (J.R. van Ommen).

https://doi.org/10.1016/j.cej.2024.149100
Received 16 November 2023; Received in revised form 12 January 2024; Accepted 23 January 2024
Available online 27 January 2024

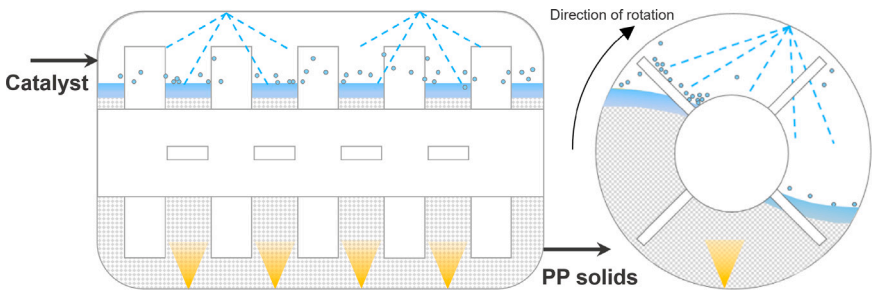

Fig. 1. Schematic representation of the front view (left) and side view (right) of the horizontal stirred bed reactor as employed in the Innovene PP process. The PP solids are continuously agitated, while gaseous propylene is introduced from the bottom of the reactor and liquid propylene quench is sprayed from the top.

In the Innovene process heat removal is facilitated by spraying recycled liquid propylene onto the PP powder bed from several axial positions along the length of the reactor. Upon contact with the active PP, the liquid vaporizes, absorbing the heat generated by the highly exothermic polymerization reaction and thereby cooling the system. Adequate solids circulation is necessary to achieve uniform wetting to attain a uniform bed temperature.

Significant research effort has been dedicated to kinetic studies of the polymerization reaction and theoretical modeling of the residence time distribution [4,7–9,13–16]. It is commonly accepted that the powder mixing pattern in an HSBR results from two transport effects: the continuously increasing powder net flow in the downstream direction caused by the particle growth, and the simultaneous stirring flows with equal intensity in the up- and downstream directions. Both together lead to a residence time distribution that can be described by three to five continuous stirred tank reactors in series [7,14].

Apart from computational modeling and residence time distribution experiments, experimental studies evaluating the hydrodynamics, or particle dynamics, in the HSBR have been very scarce in the current literature. The flow characteristics of biomass particles in a laboratory-scale HSBR were studied by experimental measurements [17] and computational modeling [18]. The axial dispersion coefficient was reported to increase with increasing rotation speed and number of blades, which was confirmed through experimentation and modeling. The granular flow patterns in a horizontal powder mixer, a system that shows similarities to an HSBR, were investigated by positron emission particle tracking in a collection of studies [19–21]. Laurent et al. [19] observed that the radial blades in horizontal mixers define axial compartments in the bed, in which loops of circulation were formed. In consecutive work, Laurent and Bridgwater [20] demonstrated that the velocity fields and axial dispersion coefficients scaled with the rotation speed, which is in good agreement with the aforementioned flow characteristics of biomass particles in a laboratory-scale HSBR [17]. Moreover, at sufficiently high reactor fill levels the agitator shaft was reported to have a dominant effect on the radial and axial particle motion [21]. Evaluating the particle dynamics is crucial for optimizing and intensifying reactor operation, as well as validating computational models. The extent of solids circulation and axial dispersion significantly influences the stability of reactor operation and the quality and uniformity of the final polymerized product. However, the hydrodynamics of multiphase flow reactors are well-known for their complexity, making their evaluation challenging. The multiphase nature of the flow in the HSBR, characterized by a large fraction of the particulate phase, makes the dense flow opaque to visible light. Consequently, the use of well-established optical techniques is hindered.

In this study, we characterize the particle dynamics in a laboratory-scale HSBR under non-reactive conditions, employing an in-house single-photon emission radioactive particle tracking (RPT) method previously introduced by van der Sande et al. [22]. Traditional RPT has emerged as a proven non-invasive technique for assessing hydrodynamic phenomena in multiphase flow systems [23–29]. It generally involves the introduction of a γ-radiation emitting tracer particle, possessing similar physical properties as the dispersed phase, into the system of interest. Subsequently, strategically positioned detectors surrounding the system enable precise reconstruction of the tracer particle's positional trajectory over time, thereby facilitating a comprehensive evaluation of hydrodynamic properties. In comparison to traditional methods, single-photon emission RPT involves reconstruction based on the photon hit location on a two-dimensional detector, mitigating the effect of varying attenuation on the reconstruction. By employing a designated calibration–experimentation procedure, van der Sande et al. [22] demonstrated reconstruction with a spatial accuracy of approximately 1 mm in controlled experiments. Moreover, the ability to study hydrodynamics in a real system was demonstrated with a case study. In the present experimental work, we employ single-photon RPT to investigate the influence of reactor operating parameters, namely reactor fill level and agitator rotation speed, on the flow field, solids circulation, and axial dispersion in a laboratory-scale HSBR.

2. Experimental and methodology

2.1. Horizontal stirred bed reactor setup

The laboratory-scale HSBR used in this work consists of a 134 mm inner-diameter cylinder with a length of 150 mm. The cylinder incorporates an agitator comprising a central shaft with seven blade positions. Each position is equipped with two blades, with each blade positioned 90° apart from its neighboring blades. The inner blades have a width of 20 mm, while the end blades have a width of 15 mm. Both the cylinder and the agitator are constructed from polycarbonate to mitigate γ-radiation attenuation during the RPT experiments. The agitator can be rotated at the desired rotation speed using an electric motor with a belt drive, which is controlled via in-house software. A schematic of the HSBR can be found in Appendix A.

To closely resemble industrial conditions, industrial-grade PP reactor powder was used in the experiments. The powder was characterized using a ZEISS SteREO Discovery.V8 optical microscope with manual 8x zoom. ImageJ software was utilized to determine the particle size distribution based on a large number of captured optical microscope images. Fig. 2 presents the number-based particle size distribution, the corresponding cumulative curve, and a typical optical microscope image of the PP powder. From the cumulative curve, it can be observed that the powder has a median diameter ($d_{n,50}$) of 1050 µm. Additionally, the loose bulk density ($\rho_{b,loose}$) of the powder was experimentally determined following the method of Carr [30] to be 368 kg m^{-3}.

2.2. Radioactive particle tracking

2.2.1. Experimental setup

The single-photon emission RPT technique utilized in this work is based on the single-photon emission computed tomography (SPECT) technique, commonly used in the medical field [31]. The RPT setup,

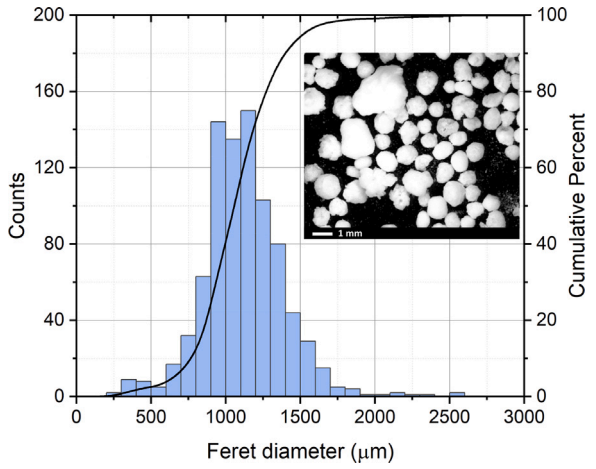

Fig. 2. Number-based particle size distribution and optical microscope image of the PP powder acquired with the ZEISS SteREO Discovery.V8 optical microscope.

recently introduced by van der Sande et al. [22], consists of three identical γ-radiation detectors that are equidistantly placed around a field of view at approximately 120° intervals, as shown schematically in Fig. 3. Each detector is composed of a casing, a slit collimator made of lead shielding plates and spacers, a scintillation crystal, and photomultiplier tubes. The setup configuration in the current experimental work has the scintillation crystal positioned at a distance of 400 mm from the collimator, allowing for the entire volume of the lab-scale HSBR to be captured. Fig. 4 shows the experimental setup with the HSBR positioned in the center of the field of view.

2.2.2. Radioactive tracer particles

In this work, two radioactive tracer particles were manufactured for calibration and experimentation purposes, respectively. The manufacturing process involved embedding 1.6 mg gold within 1.8 mm polystyrene beads. To compensate for the increased mass due to the gold core, air pockets were intentionally left within the particles. Consequently, the resulting core–shell particles had a diameter of 1.8 mm and a density of 1.65 mg cm^{-3}. With a particle diameter of 1.8 mm the tracer particle is near the upper bound of, but still within, the particle size distribution, as evident from Fig. 2, and is therefore assumed to show representative dynamics. Neutron irradiation at the TU Delft Reactor Institute was employed to activate the stable gold cores to the radioactive isotope ^{198}Au, providing an activity of 1 MBq for calibration and 27.5 MBq for experimentation purpose.

$$^{197}_{79}\mathrm{Au} + {}^{1}_{0}\mathrm{n} \longrightarrow {}^{198}_{79}\mathrm{Au} \xrightarrow[\gamma,\beta^-]{} {}^{198}_{80}\mathrm{Hg}$$

Since the isotope ^{198}Au has a relatively short half-life of approximately 2.7 days and emits 412 keV photons in its decay to ^{198}Hg, it is a preferred tracer isotope for RPT experimentation [29].

2.2.3. Reconstruction tracer particle position

When a γ-radiation emitting tracer particle is placed within the field of view, radiation that passes through the slit collimators hits the scintillation crystals. Each photon hit is recorded as an event, which has an associated xz-position, energy, and time of detection. Combining the positions of all events detected by a scintillation crystal allows for the creation of a two-dimensional projection of the incoming γ-radiation. A backward projection method is employed to reconstruct the position of the radioactive tracer particle based on its projections on the three detectors. For each detector, a plane is reconstructed using the location of the detected photon hit on the scintillation crystal and the position of the slit collimator, as schematically represented for one detector in Fig. 3. By simultaneously constructing planes for all three detectors, a unique intersection point is obtained. The coordinates of this intersection point represent the position of the radioactive tracer particle. The detector configuration and stochastic nature of radiation result in a Poisson distribution of detection events. The standard deviation of the calculated tracer particle coordinates is inversely proportional to the square root of the sampling time, which is directly proportional to the number of detected events [32]. Increasing the activity of the tracer particle increases the number of detected events, and thus decreases the standard deviation of the calculated coordinates.

The single-photon emission RPT experimental procedure involves two successive steps (Fig. 5): (1) setup calibration using the 1 MBq tracer; and (2) trajectory reconstruction using the 27.5 MBq tracer. The calibration of the setup's geometry is performed to ensure accurate reconstruction of the tracer particle position. The calibration process aims to correct errors in the spatial geometry of the setup arising from manual measurements. This is achieved by minimizing the sum of residuals squared for a large number of known tracer particle positions and their corresponding reconstructed positions, utilizing a constrained non-linear least-squares optimization algorithm in MATLAB. The output of this algorithm provides calibrated geometry values, encompassing the spatial orientation of the detectors. The calibrated geometry values replace the initial hand-measured values and are employed in the subsequent trajectory reconstruction step. In the trajectory reconstruction step the tracer particle is added to the HSBR and its trajectory is monitored.

The reconstruction sampling time, i.e. the time between consecutive reconstructions, is directly related to the count rate detected by the detector, which in turn is a function of the source activity and distance to the detector. With the current tracer activity of 27.5 MBq, a sampling time of 100 ms was attained throughout the experiments. A sampling time of 100 ms, which equates to 10 reconstructions each second, was proven sufficient to capture small spatial steps in the trajectory of the tracer particle [22]. Relating the number of detected events used in each reconstruction at a sampling time of 100 ms to the controlled validation experiments reported by van der Sande et al. [22], a spatial accuracy of approximately 5 mm is expected. A more detailed description of the experimental procedure and discussion on the reconstruction is described in our previous work [22].

Table 1
Experimental operating conditions investigated. Each possible combination of the fill level and rotation speed is studied.

Parameter	Value		
Fill level (v%)	40	50	60
Rotation speed (RPM)	20	40	60

2.3. Operation and flow characterization

During the operation of the HSBR in industrial applications, the bed level is kept at constant inventory and the rotation speed is kept constant. Adequate control of the fill level and rotation speed is necessary to prevent operational issues, as these have a significant influence on the particle dynamics in rotating systems [21,33]. To comprehend the influence of both aforementioned parameters on the particle dynamics in the HSBR, an experimental parameter study was performed. The set of operating conditions is denoted in Table 1.

For each experiment, the HSBR was loaded with the desired fill level by inserting PP powder through the top opening. Subsequently, the 27.5 MBq tracer was added to the HSBR. The agitator rotation speed was then set to the desired value using in-house software. After 10 s the RPT detectors were switched on and the trajectory of the tracer particle was monitored for a duration of 20 min. Since the rotation speeds used in this study vary between 20 RPM to 60 RPM, the reactor agitator has made between 400 to 1200 rotations during a 20 min measurement, which is assumed sufficient for reliable data interpretation. From the obtained data set the particle dynamics in the HSBR were characterized and analyzed.

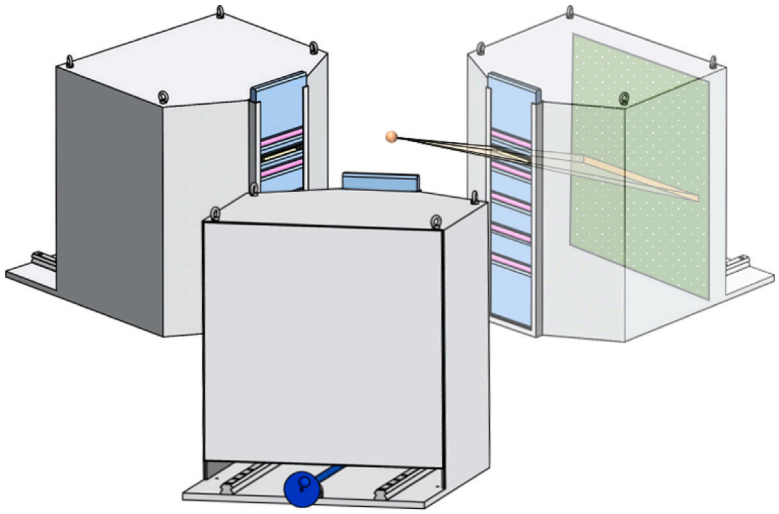

Fig. 3. Schematic of the RPT setup showcasing the three detectors placed equidistant with a 120° angle. The γ-radiation emitted by a radioactive tracer particle passes through the slit collimators and hits the scintillation crystals.

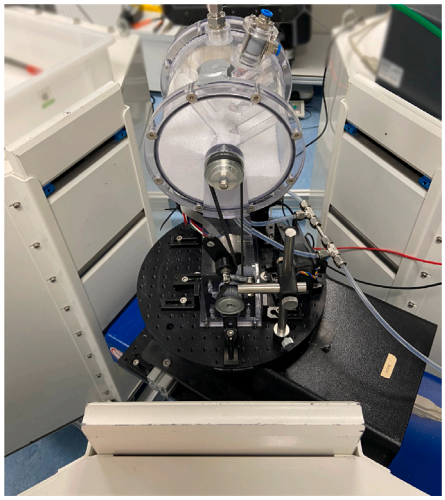

Fig. 4. Photograph of the experimental setup. The HSBR loaded with PP powder is positioned in the center of the RPT setup, comprising three γ-radiation detectors.

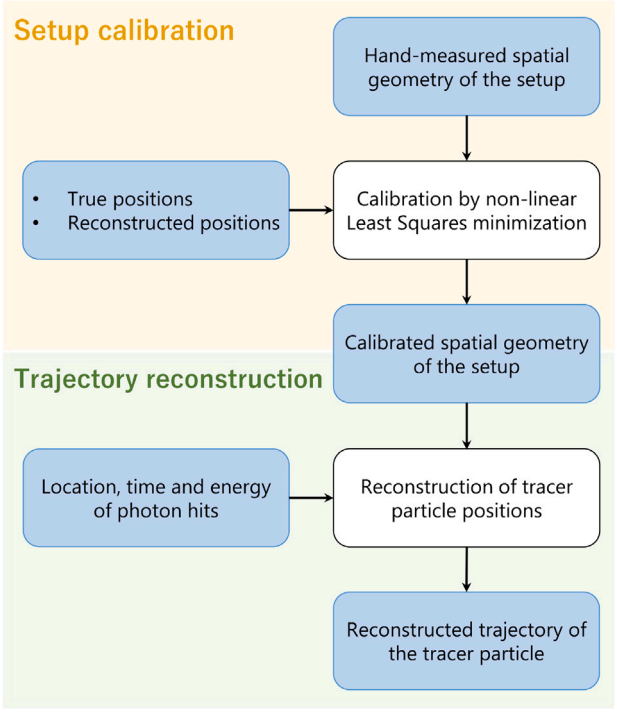

Fig. 5. Graphical representation of the experimental and data processing workflow to reconstruct the trajectory of the tracer particle, following a subsequent calibration and experimentation step.

2.3.1. Solids flow field

The obtained particle trajectory was used to evaluate the solids flow field in the xz-plane (see Fig. 6 for a definition of the coordinate system). The particle velocity was computed from the time-resolved tracer particle positions by

$$v_{i,j}(t) = \frac{X_i(t_j + \Delta t) - X_i(t_j)}{\Delta t} \quad (1)$$

To compute the velocity heat map, a mesh-grid function in MATLAB was used to create a rectangular grid of the HSBR xz-plane. The flow velocity at each grid cell was computed by triangulation-based natural neighbor interpolation. Following a similar procedure, the velocity vectors were normalized and interpolated to compute the direction of the flow.

2.3.2. Solids circulation

The particle dynamics in an HSBR are dominated by continuous agitation, which induces particle circulation. Slow and irregular particle circulation is undesirable in industrial operation, as it may lead to the formation of hot spots due to insufficient and irregular heat dissipation, potentially causing agglomeration and impairing reactor efficiency. In contrast, fast particle circulation allows for more frequent particle wetting, thereby improving the uniformity of the bed.

The particle circulation behavior in the experimental HSBR can be directly characterized by the obtained trajectory of the tracer particle. To quantify the particle circulation behavior, a cycle time is defined as the time it takes for a particle to make a full circumferential cycle. An in-house MATLAB script was used to determine the number of cycles and respective cycle times for each experiment.

2.3.3. Solids axial dispersion

Since RPT allows the trajectory of a tracer particle to be obtained, the axial dispersion can be evaluated from Einstein's expression [34].

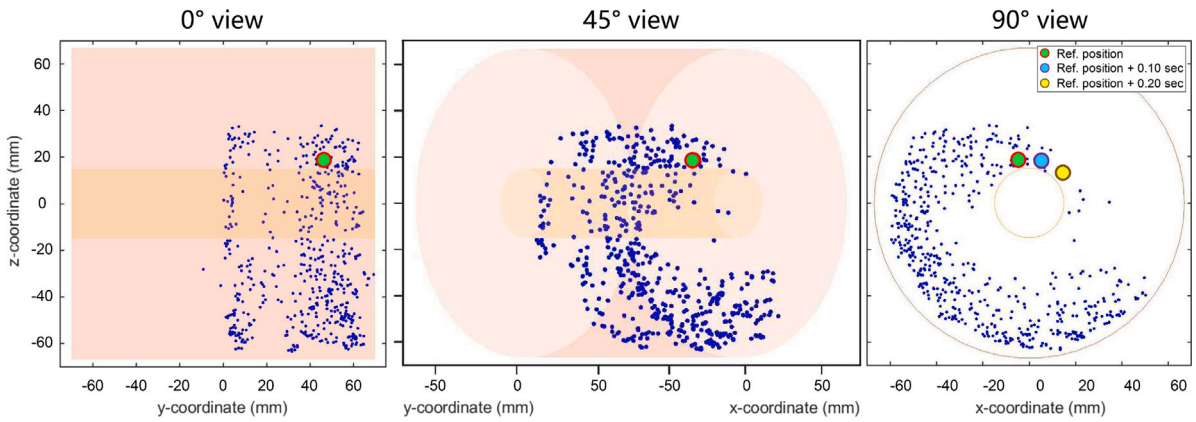

Fig. 6. Reconstructed positions of the tracer particle accumulated for a time period of 1 min for a fill level of 50% and rotation speed of 40 RPM. The instantaneous position is referenced by the red-outlined green dot. Two consecutive reconstructed positions are indicated in the 90° view. The reactor wall and agitator shaft are indicated with a red and orange color, respectively.

The local particle dispersion (D_y) coefficient is calculated with a method derived from Mostoufi and Chaouki [26] and Pallarès and Johnsson [35]. The axial displacement during a time interval Δt is

$$\Delta y_{i,j} = y_i(t_{j+1}) - y_i(t_j) \tag{2}$$

$$t_j = t_0 + j\Delta t \tag{3}$$

The mean displacement can then be defined as

$$\bar{\Delta y} = \frac{1}{N_t}\frac{1}{N_p}\sum_{j=1}^{N_t}\sum_{i=1}^{N_p}\Delta y_{i,j} \tag{4}$$

where N_t is the number of time steps and N_p is the number of particles. The axial dispersion coefficient, $D_{y,i,j}$, of a single particle at a certain time-step is then computed as

$$D_{y,i,j} = \frac{(\Delta y_{i,j} - \bar{\Delta y})^2}{2\Delta t} \tag{5}$$

Finally, the coefficients are averaged over the experiment duration to obtain the time-averaged axial dispersion coefficient

$$D_y = \frac{1}{N_t}\sum_{j=1}^{N_t} D_{y,j} \tag{6}$$

As emphasized by Pallarès and Johnsson [35], careful consideration of the time interval value (Δt) holds significant importance when computing the axial dispersion coefficient. Setting Δt at a very low scale (around 10^{-1} s or even lower) results in the dispersion coefficient not aligning well with the observed trajectory [35]. Conversely, when opting for considerably high Δt values, there is a risk of exceeding the characteristic time for axial transport, resulting in a loss of valuable information. To determine the most suitable Δt to be used in this work, the influence of the Δt on the calculated value of the axial dispersion coefficient was studied by calculating the axial dispersion coefficient values using a wide range of Δt values. The results are presented in Appendix B. It can be observed that at a very low scale, the axial dispersion quickly decreases until a plateau is reached for a Δt larger than 5 s. Moreover, for a Δt of 30 s or larger, the calculated axial dispersion coefficients for different experimental conditions approach each other, hinting that valuable information that allows distinction between experimental conditions might be lost. Therefore, a Δt of 10 s was considered suitable and was consequently employed in the evaluation of the axial dispersion.

3. Results and discussion

3.1. Time-resolved trajectory

For each set of operating conditions, the trajectory of the 27.5 MBq tracer particle within the HSBR was reconstructed over a time period of 20 min with a sampling time of 100 ms. Fig. 6 presents the particle trajectory for a 1 min time period for a reactor fill level of 50% and a rotation speed of 40 RPM, providing 0°, 45°, and 90° angle views to show the three-dimensional nature of the reconstruction. The blue scatter markers represent distinct reconstructed positions accumulated during the specified time interval. A video showing the time-resolved trajectory is included in Appendix C. In the 90° angle view three consecutive reconstructed positions of the tracer particle are exhibited: the instantaneous reference position, the reference position after 0.1 s, and the reference position after 0.2 s. The relatively small spatial step between these consecutive reconstructed positions underscores the adequacy of the 100 ms sampling time for accurately tracing the tracer particle's path within the HSBR at a rotation speed of 40 RPM.

3.2. Solids flow field

The solids flow fields were computed via the aforementioned grid interpolation procedure and are shown for the xz-plane in Fig. 7. When considering the flow velocity, two regions can be distinguished in each plot, namely a low velocity (cold color) region at the bottom and left side of the bed and a high velocity (warm color) region at the top and right side of the bed. At the bottom and left side of the bed, the agitator is the driving force for the motion of the bed material, yielding uniform solids dynamics with a low velocity. In the current work, the rotation speed was varied from 20 to 60 RPM, which corresponds to a Froude number varying from 0.03 to 0.28. A Froude number below 1 means that the gravitational force is dominant over the inertia force, indicating that the flow behavior of the bed is influenced by the force exerted by the impeller blades, frictional forces on the wall, shear forces, and gravity [36]. In contrast to the bottom and left side of the bed, at the top and right of the bed material flows freely over the shaft and gravity is the driving force for the downward motion of the bed material. This region is characterized by higher flow velocities. As expected, it can be observed that the flow velocity is increased in both regions with increasing agitator rotation speed.

Notable observations are made when comparing the solids flow field for the various experimental conditions. From the flow fields, local circulation under the shaft can be observed for the cases of 40% fill level with a rotation speed of 20 and 40 RPM. The particles that experience local circulation are less likely to reach the top of the bed. This behavior would be highly undesirable from an application point of view, as it may result in large temperature gradients in the bed due to poor heat dissipation. However, a further increase in rotation speed to 60 RPM results in the expansion of the bed. Such expansion or aeration at increased rotation speeds is commonly encountered in rotating drum reactors [37], and in this case allows a significant part

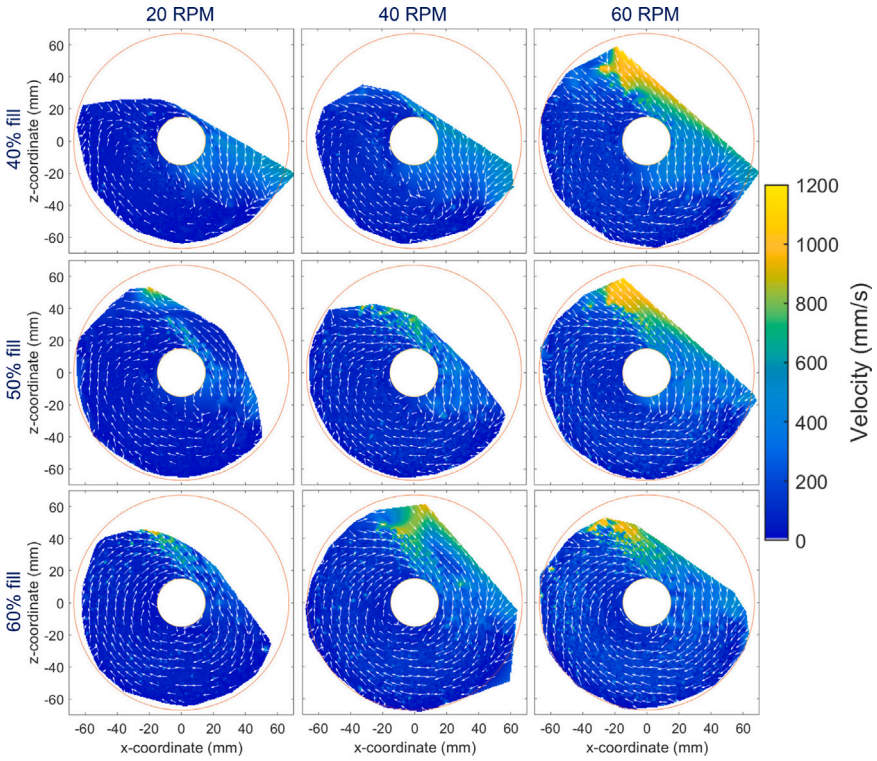

Fig. 7. Projection of the time-averaged tracer velocity heat maps and flow direction quiver plots in the xz-plane averaged over the y-axis.

of the bed to flow over the shaft, thereby significantly improving the circumferential motion. Nonetheless, internal circulation under the shaft can still be observed. Increasing the reactor fill level from 40% to 50% improves the circumferential motion and reduces the internal circulation. Notably, no internal circulation is observed at a reactor fill level of 50% and a rotation speed of 60 RPM, indicative of excellent circumferential solids motion. Consistent findings are evident across various rotation speeds when the fill level is maintained at 60%.

These findings align closely with the observations documented by Laurent et al. [36], who noted the presence of a circulation loop beneath the agitator shaft in a horizontal powder mixer operated at low fill levels. This phenomenon was attributed to a substantial portion of the bed flowing underneath the shaft. Conversely, at higher fill levels, the shaft compelled the powder to flow over it, preventing the formation of a circulation loop. Laurent et al. [36] observed the most notable change in flow behavior between fill levels of 40% and 50%, correlating with the splitting of material by the shaft. Some material was found to flow over the shaft, while the rest was found to flow beneath it, forming a circulation loop. As discussed, the same phenomenon is also visible for distinct cases in Fig. 7. Interestingly, despite the difference in design and configuration of the agitator among horizontal powder mixers and an HSBR, the most notable change in flow behavior was also observed to occur between 40% and 50% fill level in this work, which is attributed to the flow over the shaft.

Fig. 8 quantitatively presents the solids velocity as a box plot for the various operating conditions. In agreement with the flow field profiles (Fig. 7), the solids velocity shows an increase for both an increase in rotation speed and reactor fill level. More specifically, it can be observed that the mean velocity has a linear relationship with the rotation speed. In addition, it is interesting to relate the solids velocity directly to the tip speed of the impeller blades by dividing the mean velocity, shown in Fig. 8, by the respective impeller tip speed, shown in Table 2. The obtained results are plotted in Fig. 9.

It can be observed that the ratio of the mean tracer particle velocity to the tip speed decreases with an increasing rotation speed for all tested reactor fill levels. It is evident that, across all rotation speeds,

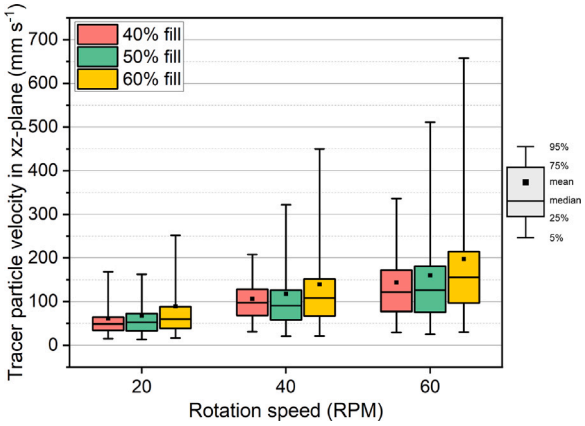

Fig. 8. Influence of the fill level and rotation speed on the flow velocity distribution of the tracer particle in the xz-plane.

Table 2
Impeller tip speed at the various rotation speeds.

Rotation speed (RPM)	Tip speed (mms^{-1})
20	140.3
40	280.6
60	421.0

the highest value is obtained for a reactor fill level of 60%. For a fill level of 60% and a rotation speed of 20 RPM, the mean speed of the tracer particle is approximately 0.63 times the tip speed of the impeller blades. When increasing the rotation speed, the ratio decreases quickly at first but then appears to stabilize at higher rotation speeds. The 40 and 50% fill levels show a similar decreasing trend with increasing rotation speed. This observation is further supported by additional experiments for a larger set of experimental conditions presented in Appendix D. Overall, the results show that increasing the rotation speed

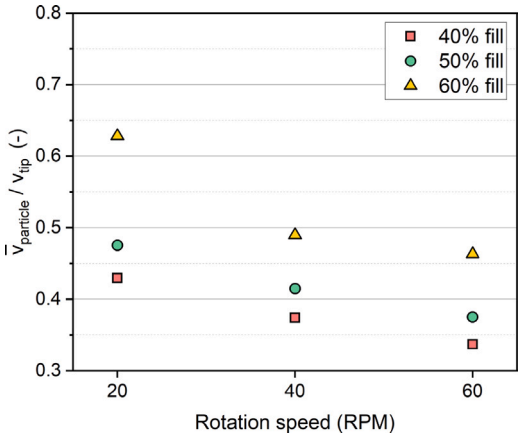

Fig. 9. Influence of the fill level and rotation speed on the ratio of the mean particle velocity to the impeller blade tip speed.

of the impellers has diminishing returns on the mean velocity of the tracer particle. Increasing the rotation speed increases the mean tracer particle velocity by a fraction, which in turn decreases with increasing rotation speed.

3.3. Solids circulation

The normalized radial occupancy over a time period of 20 min is presented in Fig. 10. From the xz-plane, the circumferential and radial dispersion of the tracer particle in the reactor is visualized. Due to the clockwise rotation of the agitator, the granular bed is mixed in a clockwise manner, resulting in the left side of the bed being pushed upward and flowing over the shaft. A clear distinction can be made between cases with poor distribution and good distribution. Notably, when the reactor is operated with a fill level of 40% at rotation speeds of 20 and 40 RPM, the radial distribution of the tracer particle throughout the bed is poor, indicated by the presence of zones with high normalized occupancy (dark blue color) and low normalized occupancy (light blue to white color). It is important to note that the plots concern normalized occupancy. If the particle resides at a certain preferred radial position for a longer duration, which is the case for operation at 40% fill level at 20 and 40 RPM, it results in a dark blue-colored region. Operation with a low fill level and low rotation speed results in a flowing regime that is characterized as a semi-static bed, in which solids motion is induced only by the passage of an impeller blade. In agreement with the flow fields presented in Fig. 7, it appears that under these operating conditions the tracer particle experiences predominantly internal circulation in a region under the shaft. As mentioned earlier, the tracer particle size is near the upper bound of the particle size distribution of the PP powder. It can be observed that with the aforementioned operating conditions the flow behavior results in poor radial solids dispersion of solids in the bed and potentially results in size segregation, which is highly undesirable from an industrial application point of view.

On the contrary, when the reactor is operated with a higher fill level and/or higher rotation speed, it can be observed that the normalized occupancy is uniform throughout the bed, indicative of improved solids distribution and a well-mixed bed. A clear transition is notable when the rotation speed is increased from 40 RPM to 60 RPM at a reactor fill level of 40%. In contrast to the rotation speed of 20 and 40 RPM, at a rotation speed of 60 RPM, the bed is aerated and thereby expanded. The expansion of the bed facilitates free powder flow over the shaft, improving the circumferential motion and radial dispersion. A similar observation is made when only the reactor fill level is increased from 40% to 50%, which results in improved powder flow. The bed is in a regime that can be characterized as a dynamic bed, where solids motion throughout the bed is continuous resulting in a more uniform solids distribution. The impeller blades no longer induce motion only by passing through the bed, but rather continuously transport the bed with a clockwise motion. This observation is in line with results obtained by Laurent et al. [36] and Laurent and Bridgwater [20], who studied the performance of single and six-blade powder mixers for various fill levels. They found that at a low fill level, the flow is directed only by the passage of the impeller blade through the bed, allowing the material to flow on the free surface and forming a circulation loop below the shaft. At a higher fill level, the presence of the shaft influences the flow behavior, and the bed is pushed continuously in a clockwise manner by an impeller blade as a solid plug.

To quantify the circumferential motion of the solids, a particle cycle time is defined as the time it takes for the tracer particle to flow over the shaft and complete a full circumferential cycle. In the industrial manufacturing of PP in an HSBR, a low cycle time would mean that the particle frequently passes the top of the reactor, where it is wetted by the quenching liquid and thus cooled down through evaporative cooling. Frequent wetting allows better control of the temperature of the polymerized solids and therefore a uniform temperature distribution throughout the bed. The cycle time is presented as a box plot for the various operating conditions in Fig. 11.

From the figure a trend can be observed for the agitator rotation speed and the cycle time, showing a decrease in the cycle time for an increase in agitator rotation speed. In other words, the solid circulation is increased. When the reactor is operated with a fill level of 40% at rotation speeds of 20 and 40 RPM, the cycle time is high, has a large distribution, and a high 95% value, indicative of slow circumferential motion. The large distribution is related to the large spread in cycle times and the limited number of cycles obtained for these operating conditions. The cycle time is significantly reduced for an increase in rotation speed to 60 RPM. More interestingly, it is evident that an increase in reactor fill level also leads to a decrease in cycle time, observable for each rotation speed. In agreement with previous observations made from the flow field and the normalized radial occupancy, the increase in reactor fill level leads to improved powder flow, enhancing the circumferential motion of solids.

To further elucidate the relation between rotation speed and cycle time, a dimensionless cycle number is proposed. The cycle number is defined as the ratio of the number of particle cycles per unit time to the number of agitator rotations per unit time, as denoted in Eq. (7). The cycle number for the various operating conditions is plotted in Fig. 12.

$$Cycle\ number = \frac{\#\ particle\ cycles\ per\ unit\ time}{\#\ agitator\ rotations\ per\ unit\ time} \tag{7}$$

It can be observed that a reactor fill level of 40% results in a cycle number that remains constant at a value of 0.1 for a rotation speed of 20 and 40 RPM, meaning that a tracer particle makes 0.1 cycles for each revolution of the agitator. In line with earlier observations, a clear jump is observed when the rotation speed is increased to 60 RPM. At a fill level of 50%, the cycle number remains constant for the various rotation speeds at a value of approximately 0.55, indicating a linear relationship between the cycle time and the rotation speed. When further increasing the fill level to 60%, the cycle number is increased. Interestingly, the cycle number has a maximum value of approximately 1.1 at a rotation speed of 20 RPM, indicative of solid circulation faster than the agitator rotation. In this case, the particle moves with the same angular velocity as the impellers in a large part of the bed and is likely to overtake an impeller blade during the free flow over the shaft, as expected from the velocity profile in Fig. 7. The finding is in agreement with observations made from the presented particle velocity results in Fig. 9.

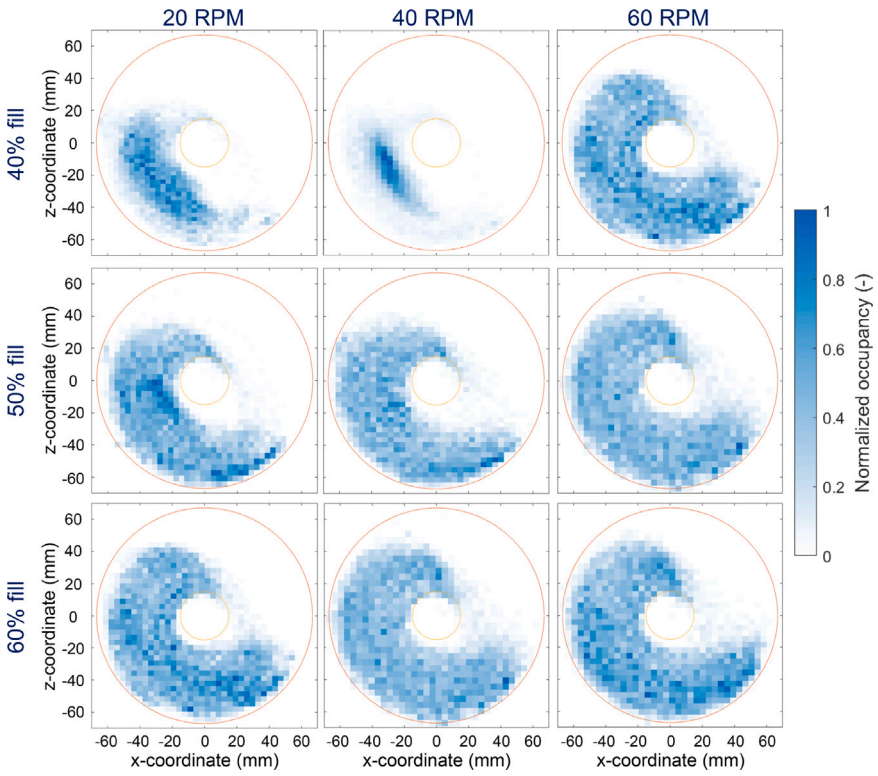

Fig. 10. Influence of the fill level and rotation speed on the tracer particle normalized radial occupancy. In each plot, the HSBR shaft is indicated by the yellow outlined circle.

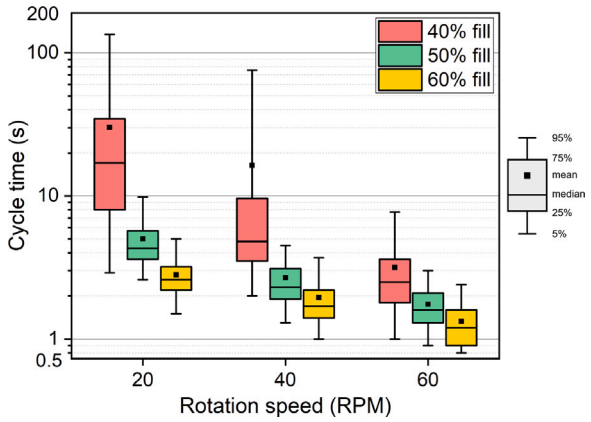

Fig. 11. Influence of the fill level and rotation speed on the cycle time distribution of the tracer particle.

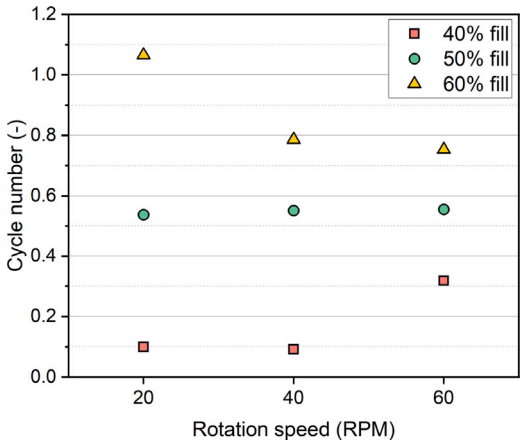

Fig. 12. Influence of the reactor fill level and rotation speed on the dimensionless cycle number, representing the number of particle cycles per full revolution of the agitator.

3.4. Solids axial dispersion

The normalized axial occupancy over a time period of 20 min is presented in Fig. 13. From the xy-plane, the axial dispersion of the tracer particle in the reactor is visualized. Since the impellers are straight, and there is no external driving force for axial transport, the axial motion of the tracer particle is considered to be random, meaning that when a particle is lifted by an impeller blade it has an equal chance to flow to the left or right of the impeller.

In the figure, a clear distinction can be made between cases with low and high axial distribution. When the reactor is operated with a fill level of 40% at rotation speeds of 20 and 40 RPM the axial dispersion of the tracer particle throughout the bed is low, indicated by small areas with a high normalized occupancy (dark blue color). As described earlier, at the aforementioned operating conditions there is significant internal bed circulation and poor circumferential solids motion. It is evident from Fig. 13 that this behavior results in a low degree of axial dispersion. On the other hand, when the powder flow is improved due to an increase in rotation speed and reactor fill level, the axial dispersion throughout the reactor is increased. The latter observation is evident from the significant axial movement the tracer particle shows through the HSBR, as it is reconstructed at nearly each coordinate value along the *y*-axis. In addition, the normalized occupancy is increasingly more uniform and has a higher coverage with increasing reactor fill level and rotation speed.

Next to the solids hold-up, it is interesting to study the dynamics of the axial dispersion. The temporal evolution of the axial position of the tracer particle is illustrated in Fig. 14 for the various operating conditions. In agreement with previously discussed results, a clear distinction can be observed between the experiments with a 40% fill level operated at 20 and 40 RPM and the rest of the measurements.

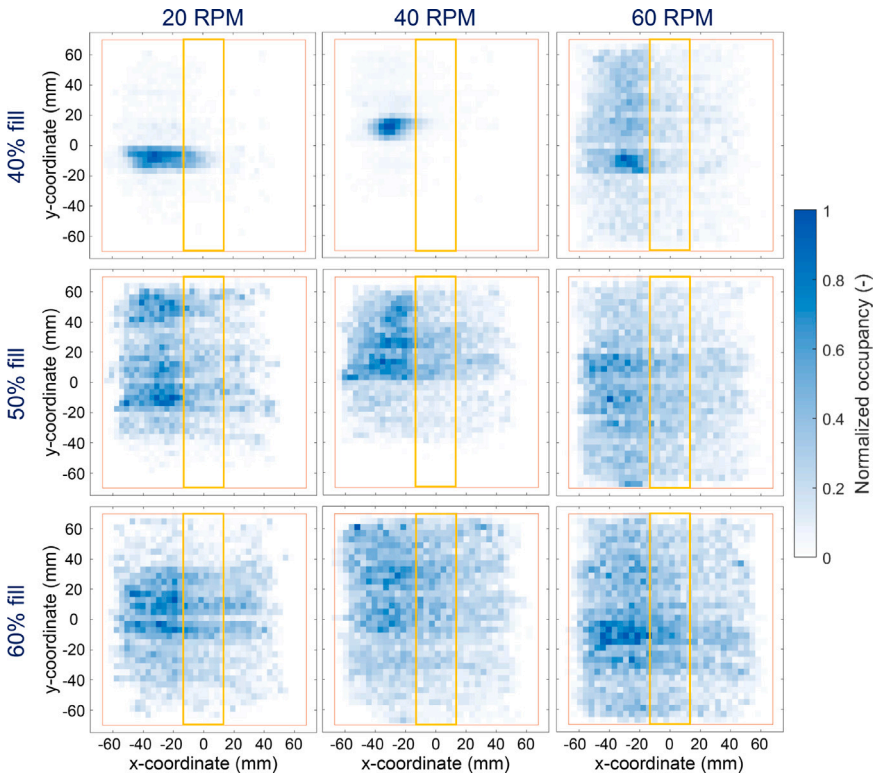

Fig. 13. Influence of the fill level and rotation speed on the tracer particle normalized axial occupancy. In each plot, the reactor shaft is indicated by the yellow-outlined rectangle.

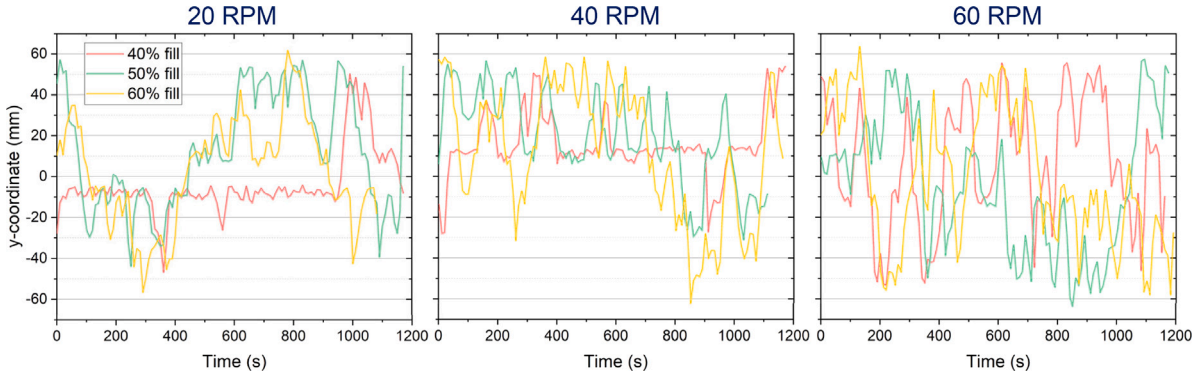

Fig. 14. The temporal evolution of the axial position of the tracer particle as a function of the reactor fill level and rotation speed.

When the HSBR is operated at the former operating conditions, the tracer particle shows significantly less axial motion compared to the other operating conditions.

As described in Section 2.1, the HSBR incorporates an agitator comprising a central shaft with seven blade positions. Each position is equipped with two blades, with each blade positioned 90° apart from its neighboring blades. The blade configuration in the HSBR appears to induce 'conveyor belt' compartments in the bed at low reactor fill levels and rotation speeds, in which particles circulate at a fixed axial position for a certain residence time. A particle, or cluster of particles, may reside for tens of seconds up to several minutes within one compartment before it moves to another compartment. The compartments are not recognized for higher reactor fill levels and/or rotation speeds, as visible in Fig. 14. Although a zone with high normalized occupancy is visible in the solids hold-up profile for a fill level of 40% and rotation speed of 60 RPM at the y-coordinate −20 mm, it is evident from the temporal evolution that this is not caused by the particle residing in a 'conveyer-belt' compartment over a long time period. Rather, the particle frequently resides at, or passes, this axial position for a short time period. When accumulating a large number of short time periods at a certain axial position, it results in a high normalized occupancy. In contrast to our findings, Laurent and Bridgwater [20] observed axial compartments defined by the radial supports on which the blades are fixed at all fill levels, ranging from 20% to 60%, in horizontal powder mixers. However, the difference is likely attributed to the difference in the system design, in particular the configuration of the agitator.

The time-averaged axial dispersion coefficient is plotted in Fig. 15. It can be observed that the axial dispersion coefficient ranges from 10^{-6} to 10^{-5} $m^2\,s^{-1}$. Moreover, the results clearly show that the axial dispersion coefficient increases with increasing rotation speed, which is in line with findings of Laurent and Bridgwater [21], Portillo et al. [33] and Xi et al. [17], who studied the axial dispersion in comparable powder agitating systems. In this work, the lowest values are found for the measurements with 40% fill level operated at 20 and 40 RPM. Interestingly, the highest extent of axial dispersion is obtained for a reactor fill level of 40% and a rotation speed of 60 RPM. Under these operation conditions, significant bed expansion is observed, which in turn increases the circumferential motion of the solids, as is evident

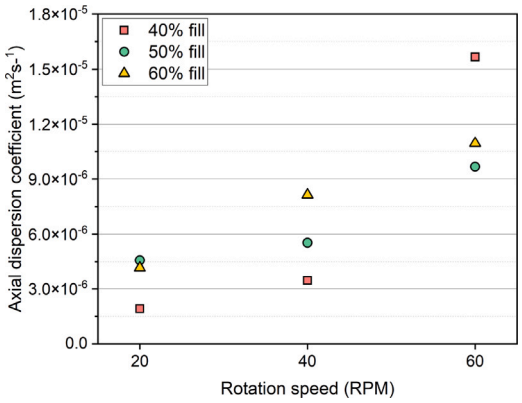

Fig. 15. The influence of the reactor fill level and rotation speed on the axial dispersion coefficient.

from the solids' hold-up profile and cycle time. At low fill levels, the solids have more free physical space to move freely during the flow over the shaft, potentially increasing their axial reach. The latter would explain the obtained higher value for the axial dispersion coefficient under these operating conditions. By comparing the observed trend with the temporal changes in the axial position of the tracer particle (depicted in Fig. 14) and the axial solids hold-up (shown in Fig. 13), it can be concluded that the trend aligns well across the obtained results.

While the literature on axial dispersion in laboratory-scale HSBRs is very scarce, significant attention has been given to studying axial dispersion in rotating drums through numerical simulations and experimental investigations. Notably, axial dispersion coefficients have been documented for rotating drums at approximately 10^{-6} $m^2\,s^{-1}$ [38], a value that corresponds well with or is slightly below the coefficients showcased in Fig. 15. The minor difference between the values in a rotating drum and the HSBR could be attributed to their different configurations. The HSBR comprises an agitator, which potentially leads to increased axial movement when compared to a rotating drum.

An additional common observation concerning rotating drums is the linear correlation between the axial dispersion coefficient and the rotation speed. It is important to note that drawing a direct comparison to this work was challenging due to the narrower range of rotating speeds in rotating drums typically encountered in the literature, usually spanning from 5 to 15 RPM [38,39]. Studies showed that the axial dispersion coefficient in rotating drums is influenced by the fill level. Namely, it was demonstrated that a higher fill level corresponds to a lower axial dispersion coefficient [38]. This particular effect is not discernible across all operating conditions for the laboratory-scale HSBR, as evident from Fig. 15. In this work, it was demonstrated that an increase in fill level results in increased powder flow, which in turn results in a lower particle cycle time. When the bed material flows over the shaft more frequently, it could potentially facilitate increased axial transport in the process. However, an increased fill level also reduces the free space in the reactor, potentially decreasing the flowing path length of the particles and thereby limiting axial transport. These two conflicting mechanisms result in an inconclusive relationship between the fill level and the axial dispersion coefficient in the HSBR.

4. Conclusions

In the current work, a quantification of the particle flow dynamics in a non-reactive laboratory-scale horizontal stirred bed reactor (HSBR) is provided using single-photon emission radioactive particle tracking (RPT). The technique has been used to reconstruct the trajectory of a 27.5 MBq tracer particle in the HSBR over a time period of 20 min with a sampling time of 100 ms under various operating conditions. From the obtained reconstructed positions data set the particle dynamics were studied. The influence of two operating parameters, namely the reactor fill level and agitator rotation speed, on the flow field, solids circulation behavior, and axial dispersion has been evaluated and the following conclusions can be drawn:

- The general particle flow behavior in the HSBR is strongly affected by the reactor fill level and agitator rotation speed. At low rotation speed and low fill level, solids motion is induced only by the passing of an impeller blade, resulting in semi-static bed motion characterized by poor solids distribution. At increased fill levels and rotation speeds, continuous solids motion throughout the bed results in a uniform solids distribution.
- The solids circulation, quantified by a dimensionless cycle number, is faster with increasing reactor fill level and rotation speed.
- The axial dispersion coefficient ranges from 10^{-6} to 10^{-5} $m^2\,s^{-1}$, which is similar to or somewhat higher than values reported for rotating drums. The axial dispersion coefficient increases with increasing rotation speed. The highest extent of axial dispersion is obtained for a reactor fill level of 40% when operated at 60 RPM, but no conclusive relation between the axial dispersion coefficient and the reactor fill level was found.

The knowledge acquired from this work not only provides a further understanding of the particle dynamics in HSBRs, but can also serve as a valuable basis for optimizing, intensifying, and scaling HSBR systems for the manufacturing of high-quality polypropylene resins on an industrial scale.

CRediT authorship contribution statement

P. Christian van der Sande: Conceptualization, Methodology, Validation, Formal analysis, Investigation, Data curation, Writing – original draft, Visualization. **Evert C. Wagner:** Conceptualization, Methodology, Investigation, Writing – review & editing. **Jack de Mooij:** Methodology, Validation, Formal analysis, Investigation, Data curation, Writing – review & editing. **Gabrie M.H. Meesters:** Conceptualization, Project administration, Writing – review & editing, Supervision. **J. Ruud van Ommen:** Conceptualization, Project administration, Writing – review & editing, Supervision.

Declaration of competing interest

The authors declare that they have no known competing financial interests or personal relationships that could have appeared to influence the work reported in this paper.

Data availability

Data will be made available on request.

Acknowledgments

The authors would like to thank Stefan ten Hagen for his contribution to the development of the laboratory-scale HSBR, Duco Bosma for his contribution to the manufacturing of the tracer particles, Mehmet Sarilar for the neutron activation of the tracer particles, the TU Delft Reactor Institute radiation protection service for ensuring a safe working environment, and Kaiqiao Wu for his contributions to the data processing.

This work was carried out as part of the 'Industrial Dense Granular Flows' project, which received funding from the Dutch Research Council (NWO) in the framework of the ENW PPP Fund for the top-sectors and from the Ministry of Economic Affairs in the framework of the 'PPS-Toeslagregeling'.

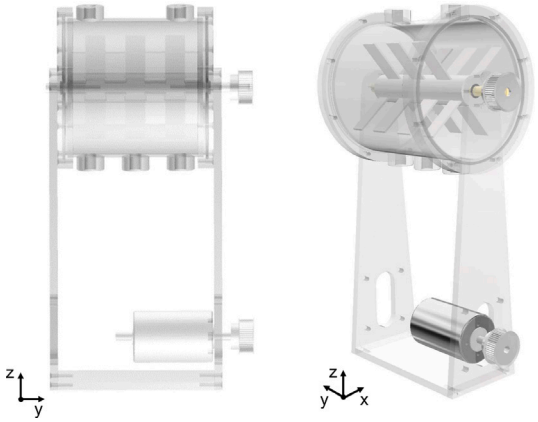

Fig. A.1. Schematic representation of the laboratory-scale horizontal stirred bed reactor. The x-y-z origin is defined in the center of the HSBR cylinder.

Appendix A. Schematic of the laboratory-scale horizontal stirred bed reactor

Fig. A.1 shows a schematic representation of the laboratory-scale horizontal stirred bed reactor used in this work. The reactor consists of a 134 mm outer-diameter cylinder with a length of 140 mm and incorporates an agitator comprising a central shaft with seven blade positions. Each position is equipped with two blades, with each blade positioned 90° apart from its neighboring blades. The inner blades have a width of 20 mm, while the end blades have a width of 15 mm. The agitator can be rotated at the desired rotation speed using an electric motor with a belt drive, which is controlled via in-house software.

Appendix B. Axial dispersion time-step

As elaborated on in Section 2.3, the axial dispersion coefficient, $D_{y,i,j}$, of a single particle at a certain time-step, is computed as:

$$D_{y,i,j} = \frac{(\Delta y_{i,j} - \bar{\Delta y})^2}{2\Delta t} \tag{8}$$

Fig. B.1 demonstrates how the time-step, Δt, influences the computed value of the axial dispersion coefficient for a wide range of time-step values. At low time-step values, the axial dispersion decreases rapidly until a plateau is reached beyond a Δt of 5 s. When Δt exceeds 30 s, dispersion coefficients for various experimental conditions converge, indicating a loss of potential information that is unique to a specific experimental condition. Considering both extremes, a Δt of 10 s was deemed appropriate and was therefore used in the calculations of the axial dispersion coefficient in this work.

Appendix C. Video reconstructed trajectory

Video C.1 presents the trajectory of the 27.5 MBq tracer particle through the HSBR operated at a fill level of 50% and a rotation speed of 40 RPM for a 1 min time period. The reconstruction is performed with a sampling time of 100 ms. The projected area is rotating to demonstrate the three-dimensional nature of the reconstruction.

Appendix D. Tracer particle velocity

Fig. D.1 presents supporting experimental results that show the influence of the fill level and rotation speed on the ratio of the mean particle velocity to the impeller tip speed for a large number of experimental conditions. In close agreement with Fig. 9, a trend can be observed where the ratio of the mean tracer particle velocity to the tip speed decreases with an increasing RPM for all tested reactor fill levels. More interestingly, for an increasing rotation speed, the ratio decreases quickly at first but then stabilizes at higher rotation speeds. It should be noted that the supporting data set was acquired for a minimum of 100 agitator rotations per experiment, i.e. a measurement time of 600 s for a rotation speed of 10 RPM and 100 s for a rotation speed of 60 RPM. Due to the reduced measurement time, the supporting data has less statistical confidence, and absolute values may therefore also deviate from the 20 min experiments presented throughout this work.

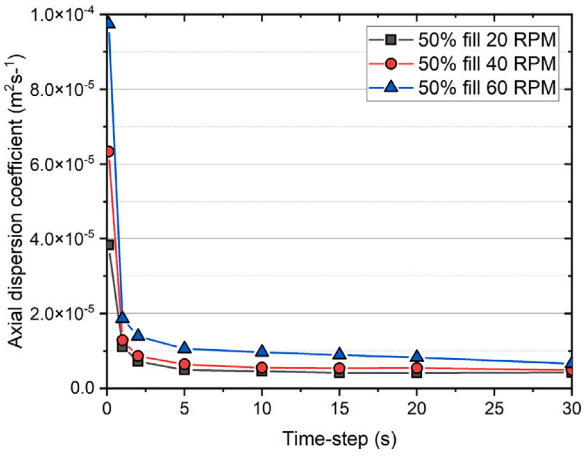

Fig. B.1. Supporting information for Section 2.3 demonstrating the influence of the time-step, varied from 0.1 to 30 s, on the computed value of the axial dispersion coefficient for operating conditions with a fill level of 50% and rotation speed of 20, 40, and 60 RPM. Based on the plots, a time-step of 10 s was deemed appropriate in the calculations since the axial dispersion coefficient is at a plateau and the coefficients for various experimental conditions have not converged.

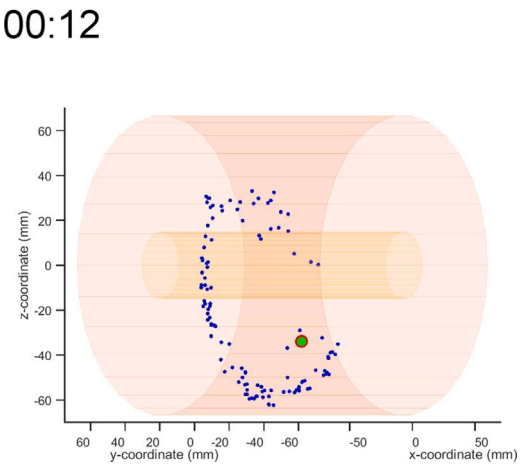

Fig. C.1. Still of the tracer particle trajectory for a fill level of 50% and rotation speed of 40 RPM. The instantaneous position is indicated by the red-outlined green dot and the blue scatter markers represent distinct reconstructed positions accumulated during the specified time interval.

Appendix E. Supplementary data

Supplementary material related to this article can be found online at https://doi.org/10.1016/j.cej.2024.149100.

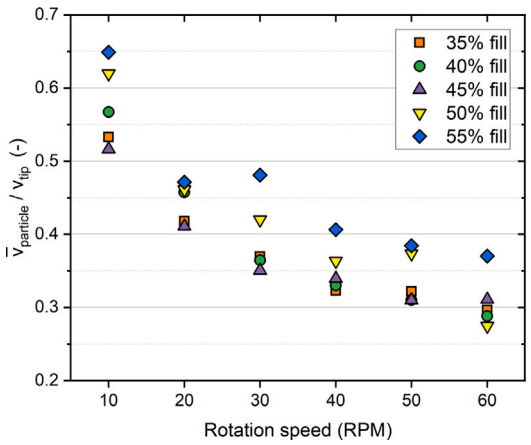

Fig. D.1. Supporting information for Section 3.2 demonstrating the influence of the fill level and rotation speed on the ratio of the mean particle velocity to the impeller blade tip speed. The data was acquired from an additional extended experimental data set, comprising a larger number of experimental conditions.

References

[1] J. Karger-Kocsis, T. Bárány, Polypropylene Handbook Morphology, Blends and Composites: Morphology, Blends and Composites, 2019, http://dx.doi.org/10.1007/978-3-030-12903-3.

[2] K. Kulajanpeng, N. Sheibat-Othman, W. Tanthapanichakoon, T.F.L. McKenna, Multiscale modelling of multizone gas phase propylene (co)polymerization reactors—A comprehensive review, Can. J. Chem. Eng. 100 (9) (2022) 2505–2545.

[3] F.B. Insights, Polypropylene Market Size, Share & Trends, Report, 2020, URL: https://www.fortunebusinessinsights.com/industry-reports/polypropylene-pp-market-101583.

[4] J.J. Zacca, J.A. Debling, W.H. Ray, Reactor residence time distribution effects on the multistage polymerization of olefins—I. Basic principles and illustrative examples, polypropylene, Chem. Eng. Sci. 51 (21) (1996) 4859–4886.

[5] J. Shepard, J. Jezl, E. Peters, R. Hall, Divided horizontal reactor for the vapor phase polymerization of monomers at different hydrogen levels. U.S. Patent 3 957 448, May 1976.

[6] J. Jezl, E. Peters, R. Hall, J. Shepard, Process for the vapor phase polymerization of monomers in a horizontal, quench-cooled, stirred-bed reactor using essentially total off-gas recycle and melt finishing. U.S. Patent 3 965 083, June 1976.

[7] M. Caracotsios, Theoretical modelling of Amoco's gas phase horizontal stirred bed reactor for the manufacturing of polypropylene resins, Chem. Eng. Sci. 47 (9) (1992) 2591–2596.

[8] A.B. Gorbach, S.D. Naik, W.H. Ray, Dynamics and stability analysis of solid catalyzed gas-phase polymerization of olefins in continuous stirred bed reactors, Chem. Eng. Sci. 55 (20) (2000) 4461–4479.

[9] C.J. Dittrich, S.M.P. Mutsers, On the residence time distribution in reactors with non-uniform velocity profiles: The horizontal stirred bed reactor for polypropylene production, Chem. Eng. Sci. 62 (21) (2007) 5777–5793.

[10] R.A. Hutchinson, Modelling of Particle Growth in Heterogeneous Catalyzed Olefin Polymerization (Ph.D. thesis), 1990.

[11] C. Bleek, M.-O. Coppens, J. Schouten, Application of chaos analysis to multiphase reactors, Chem. Eng. Sci. 57 (2002) 4763–4778.

[12] J. Wang, Y. Cao, X. Jiang, Y. Yang, Agglomeration detection by acoustic emission (AE) sensors in fluidized beds, Ind. Eng. Chem. Res. 48 (2009).

[13] R.A. Hutchinson, W.H. Ray, Polymerization of olefins through heterogeneous catalysis. VII. Particle ignition and extinction phenomena, J. Appl. Polym. Sci. 34 (2) (1987) 657–676.

[14] N.P. Khare, B. Lucas, K.C. Seavey, Y.A. Liu, A. Sirohi, S. Ramanathan, S. Lingard, Y. Song, C.-C. Chen, Steady-state and dynamic modeling of gas-phase polypropylene processes using stirred-bed reactors, Ind. Eng. Chem. Res. 43 (4) (2004) 884–900.

[15] Z. Tian, X.-P. Gu, L.-F. Feng, J.-P. Corriou, G.-H. Hu, Modeling and simulation of polypropylene particle size distribution in industrial horizontal stirred bed reactors, J. Appl. Polym. Sci. 125 (2012).

[16] M.F. Atan, M. Hussain, R. Abbasi, K. M.J.H, M. Patah, Advances in mathematical modeling of gas-phase olefin polymerization, Processes 7 (2019) 67.

[17] Y. Xi, Q. Chen, C. You, Flow characteristics of biomass particles in a horizontal stirred bed reactor: Part I. Experimental measurements of residence time distribution, Powder Technol. 269 (2015) 577–584.

[18] Y. Xi, Q. Chen, C. You, Flow characteristics of biomass particles in a horizontal stirred bed reactor: Part II. Modeling studies on particle residence time distribution and axial mixing, Powder Technol. 269 (2015) 585–595.

[19] B. Laurent, J. Bridgwater, D. Parker, Convection and segregation in a horizontal mixer, Powder Technol. 123 (1) (2002) 9–18.

[20] B. Laurent, J. Bridgwater, Performance of single and six-bladed powder mixers, Chem. Eng. Sci. 57 (10) (2002) 1695–1709.

[21] B.F. Laurent, J. Bridgwater, Influence of agitator design on powder flow, Chem. Eng. Sci. 57 (18) (2002) 3781–3793.

[22] P.C. van der Sande, J. de Mooij, E.C. Wagner, G.M. Meesters, J.R. van Ommen, Single-photon emission radioactive particle tracking method for hydrodynamic evaluation of multi-phase flows, Particuology (2023) (in press).

[23] J.S. Lin, M.M. Chen, B.T. Chao, A novel radioactive particle tracking facility for measurement of solids motion in gas fluidized beds, AIChE J. 31 (3) (1985) 465–473.

[24] M. Duduković, Opaque multiphase reactors: Experimentation, modeling and troubleshooting, in: Oil & Gas Science and Technology – Rev. IFP Éditions Technip Oil & Gas Science and Technology – Rev. IFP, vol. 55, 2000, pp. 135–158.

[25] D. Moslemian, N. Devanathan, M.P. Dudukovic, Radioactive particle tracking technique for investigation of phase recirculation and turbulence in multiphase systems, Rev. Sci. Instrum. 63 (10) (1992) 4361–4372.

[26] N. Mostoufi, J. Chaouki, Local solid mixing in gas–solid fluidized beds, Powder Technol. 114 (1) (2001) 23–31.

[27] S. Roy, Radiotracer and particle tracking methods, modeling and scale-up, AIChE J. 63 (1) (2017) 314–326.

[28] S. Roy, A. Kemoun, M.H. Al-Dahhan, M.P. Dudukovic, Experimental investigation of the hydrodynamics in a liquid–solid riser, AIChE J. 51 (3) (2005) 802–835.

[29] S. Roy, F. Larachi, M.H. Al-Dahhan, M.P. Duduković, Optimal design of radioactive particle tracking experiments for flow mapping in opaque multiphase reactors, Appl. Radiat. Isot. 56 (3) (2002) 485–503.

[30] R.L. Carr, Evaluating flow properties of solids, Chem. Eng. J. 72 (1965) 163–168.

[31] B.L. Holman, S.S. Tumeh, Single-photon emission computed tomography (SPECT). Applications and potential, JAMA 263 (4) (1990) 561–564.

[32] N. Mostoufi, G. Kennedy, J. Chaouki, Decreasing the sampling time interval in radioactive particle tracking, Can. J. Chem. Eng. 81 (1) (2003) 129–133.

[33] P.M. Portillo, A.U. Vanarase, A. Ingram, J.K. Seville, M.G. Ierapetritou, F.J. Muzzio, Investigation of the effect of impeller rotation rate, powder flow rate, and cohesion on powder flow behavior in a continuous blender using PEPT, Chem. Eng. Sci. 65 (21) (2010) 5658–5668.

[34] A. Einstein, Investigations on the Theory of the Brownian Movement, Courier Corporation, 1956.

[35] D. Pallarès, F. Johnsson, A novel technique for particle tracking in cold 2-dimensional fluidized beds—simulating fuel dispersion, Chem. Eng. Sci. 61 (8) (2006) 2710–2720.

[36] B. Laurent, J. Bridgwater, D. Parker, Motion in a particle bed agitated by a single blade, AIChE J. 46 (9) (2000) 1723–1734.

[37] Q. Huang, H. Zhang, J. Zhu, Experimental study on fluidization of fine powders in rotating drums with various wall friction and baffled rotating drums, Chem. Eng. Sci. 64 (9) (2009) 2234–2244.

[38] S. Yang, K. Luo, J.W. Chew, Three-dimensional axial dispersion dynamics of granular flow in the rolling-regime rotating drum, Powder Technol. 332 (2018) 131–138.

[39] S. Yang, L. Zhang, K. Luo, J. Wei, DEM investigation of the axial dispersion behavior of a binary mixture in the rotating drum, Powder Technol. 330 (2018) 93–104.